PAPER 05-2089

CONSTRUCTION QUALITY, TEMPERATURE AND RUTTING EFFECT ON TOP-DOWN CRACKING INITIATION

Elisabete Fraga de Freitas (contact author)
Graduate Research Assistant
Department of Civil Engineering
University of Minho
Campus de Azurém
4800 058 Guimarães Portugal
phone: +351 253 510200
fax: +351 253 510217
email: efreitas@civil.uminho.pt

Paulo Pereira
Professor
Department of Civil Engineering
University of Minho
Campus de Azurém
4800 058 Guimarães Portugal
phone: +351 253 510200
fax: +351 253 510217
email: ppereira@civil.uminho.pt

Luis Picado-Santos
Associated Professor
Department of Civil Engineering
University of Coimbra
Pinhal de Marrocos
3030 290 Coimbra Portugal
phone: +351 239 797 143
fax: +351 239 797 123
email: picsan@dec.uc.pt

A. Thomas Papagiannakis
Professor
Dept. of Civil and Enviro. Engineering
Washington State University
Pullman WA, 99164-2910
Tel 509 335 4547
Fax 509 335 7632
pappa@wsu.edu

Paper reviewed for publication in the TRB journal
(Characteristics of Bituminous Aggregate Combinations to Meet Surface Requirements)

Abstract: 185 words
Text: 3598 words
5 tables & 7 figures: 3000 word equivalents
Total: 6783 words

March 2004

ABSTRACT

Top-down cracking (TDC) is a flexible pavement distress caused by a number of factors, including high contact stresses from truck tires, mix design characteristics, (e.g., binder type and aggregate gradation) and poor construction quality, (e.g., segregation and compaction methods). This paper presents the findings of a study seeking to quantify the effect of these factors on TDC. It consists of a laboratory component involving an accelerated Wheel Tracking device and a modeling component involving a 3-D non-linear viscoelastic finite element model. The laboratory component of the study involved 17 asphalt bituminous slabs, constructed to simulate the variation in material properties observed in the field as part of an earlier forensic TDC study. The effect of air voids, bitumen content and type, aggregate gradation and segregation on TDC were studied under 3 temperature conditions. Air voids, segregation and binder content were found to have a significant effect on TDC for all the temperatures tested. Modeling the TDC involved laboratory testing to establish the viscoelastic and tensile strength properties of the asphalt mixtures tested. It was found that the rutted surface contributes significantly to TDC initiation.

INTRODUCTION

Top-down cracking (TDC) is a flexible pavement distress defined by cracks begining at the surface of the asphalt concrete layer and propagating downwards with time. TDC has received relatively little attention in the literature compared to the so-called conventional traffic-associated flexible pavement distresses, such as bottom-up asphalt concrete cracking and granular layer rutting. Recently, there has been renewed interest in modeling the initiation and progression of TDC, (e.g., the new Pavement Design Guide being developed by the NCHRP study 1-37A and the on-going NCHRP study 1-42). Clearly, TDC is a distress mechanism that needs to be better understood, incorporated into pavement performance prediction models, as well as included in the systems used for managing pavements.

Literature suggests that TDC begins in the first few years of pavement life, e.g., in the first year as reported in Japan (1), although it could begin much later, e.g., in the tenth year, as reported in Florida (2). It seems to occur in a variety of asphalt concrete pavements located in a wide range of environmental conditions. Cracks appear mostly outside the wheel path, in areas exposed to extensive solar radiation (2, 3, 4). Six main factors have been reported to contribute to TDC initiation and propagation:

- climatic conditions (3, 5),
- traffic conditions, including the load and inflation pressure of truck tires (2, 6, 7),
- aging of the binder (8),
- structural conditions, including layer thickness (3, 9, 10),
- mixture properties, including binder type and aggregate gradation (1) and
- construction quality, including segregation and compaction procedures (9-12).

Nevertheless, the cause-effect relationship between each of these factors, their interaction and TDC is not clearly understood.

Preliminary work for this study involved forensic analysis of eight 80×80×30 cm asphalt slabs and forty-four cores extracted from an 8-year-old roadway pavement in the north of Portugal revealing TDC (4). Physical examination of these field samples revealed construction quality, mainly in the form of segregation, as the main cause of TDC initiation and progression. This was evident not only in the wearing course but also in the levelling courses. Aggregates were poorly graded and exhibited excessive fine particles. Void content was high and showed a large variability within each slab. Bitumen content was, on average, slightly higher than 6%. Additional in-situ deflection measurements were obtained in the Spring with a Falling Weight Deflectometer (FWD). They revealed no structural deficiencies for the traffic level at the site, i.e., maximum deflections were lower than 300 μm. Samples from the wearing course were further tested in the laboratory, involving a repetitive constant height Simple Shear Tester (SST) (11). The stiffness modulus was found to be higher than 4500 MPa at 20ºC and 10 Hz, while the phase angle was lower than 10º, suggesting significant stiffening of the wearing course through ageing. A significant reduction in modulus was observed by increasing temperature from 10ºC to 25ºC. These results provided a guideline for selecting variables to include in further evaluating TDC initiation, as described below.

OBJECTIVE-METHODOLOGY

The objective of the part of the study reported herein is to further evaluate the effect of the factors identified above on TDC initiation. These include binder type, binder content, aggregate gradation, void content, aggregate-binder adhesion and temperature. This part of the study includes a laboratory component utilizing a Wheel Tracking device and a modeling component utilizing a non-linear viscoelastic finite element model.

The laboratory component involved manufacturing 17 asphalt concrete slabs with the goal of replicating the range of conditions encountered in the field during the forensic analysis conducted earlier. Mixture design took into account project specifications and field quality control, as well as possible mitigation measures. A 50/70 penetration binder was used. Granite aggregates were used and limestone filler was added to the aggregate blend, in the necessary proportion, to obtain the three grading curves depicted in Figure 1. Curve A approaches the grading envelope average curve recommended in the field study. Curves B and C are, respectively, fine graded and coarse graded, approaching the upper and lower gradation limits of the field specification. Three levels of binder content and air voids were considered, (i.e., high, normal and low), within ranges found in the preliminary work. Control binder content was set at 5.8% according to the Duriez model (13) and the field tests previously performed. Control void content was set at 4% according to project specifications. The segregation observed in the field was also simulated in the laboratory mixtures. Two additional mixtures were produced, one with hard bitumen and another using an anti-stripping compound. These mixtures were compacted in a 75.0×55.0×7.0 cm rectangular mould using a vibratory roller compacter. Specimens were obtained by cutting them from the slabs produced in the laboratory with the required dimension. A summary of each slab's physical

properties, as well as testing temperature, are presented in Table 1. Testing temperatures were selected to be representative of the range in wearing course daily temperatures measured in the Summer in the north of Portugal.

The modeling component of the study involved a non-linear viscoelastic finite element algorithm. A number of additional laboratory tests were conducted in order to obtain the material properties required for modeling. These included stiffness, shear modulus and tensile strength of the asphalt concrete. In addition, cyclic compression tests were performed to model the viscoelastic behavior of the asphalt concrete at high temperatures.

WHEEL TRACKING TEST

There have been several studies in the literature dealing with the TDC, using accelerated loading devices. Groenendijk (6) used the accelerated loading facility LINTRACK to observe TDC behavior. The Public Works Research Institute of Japan (1) custom-developed a testing machine to evaluate the effect of mixture characteristics on TDC. Uchida (8) and Wang (14) used a device similar to the Wheel Tracking test apparatus. The former studied the effect of ageing on TCD initiation, while the latter studied TDC initiation of the deformed specimens from a micromechanics perspective.

In this study, a Wheel Tracking test apparatus was used. It is recognized that this device does not realistically replicate the horizontal contact stresses applied by tires at the surface of a pavement. This is an inherent limitation of using this device, especially because these stresses are reported in the literature as one of the main causes of TDC (2). Another variable not considered in this test is the effect of binder ageing and the resulting increase in the stiffness of the asphalt concrete.

A steel mould has been used to provided confinement to the 30.5×30.5×7.0 cm specimens. The specimens were subjected to a 0.69 kN wheel load, which corresponds to a 627 kPa pressure, traveling back and forth along the centre line. The contact area was 4.9×2.2 cm^2 and the loading period was 1.395 s. Testing was conducted at three temperatures, namely 30ºC, 40ºC and 50ºC (Table 1). The condition of the surface was monitored closely to identify the number of cycles that correspond to the initiation of surface cracks. Furthermore, the rut depth was recorded as a function of the number of axle passes. Testing was terminated when rut depth reached 1.5 cm or when 20 500 cycles were reached. Overall, it was noted that nearly all tests resulted in surface cracks, regardless of temperature and mix characteristics. The number of wheel passes to produce the first crack (*nf*) and the total number of wheel passes (*nt*) are presented in Table 2. Figure 2 shows the condition of the surface of some of the samples at the end of the test. The following sections summarize the effect on TDC of each of the analyzed factors.

Results of the Wheel Tracking Test

Temperature Effect

Temperature had a major effect on TCD initiation, as can be seen by comparing *nf* values (Table 2). The number of wheel passes corresponding to the first crack greatly decreased with increasing temperature. Figures 2 a), b) and c) show the final surface condition of the three slabs tested at 30ºC, 40ºC and 50ºC.

Void Content Effect

The results from slabs 1, 6 and 9, tested at 50ºC, demonstrate that high void content accelerates TDC initiation (Figure 2 d)). The number of wheel passes corresponding to the first crack decreased with increasing void content and the number of cracks increased with increasing void content. Tests performed at 30ºC (e.g., slab 8 and 11) and 40ºC (e.g., slab 10 and 12) first showed surface changes in slabs exhibiting higher void content.

Grading Type Effect

The effect of aggregate gradation was less pronounced than the effect of temperature and void content. Nevertheless, it was observed that the coarse gradation resulted in earlier TDC initiation than the fine one. TDC tended to initiate at the interface between coarse aggregates and binder, especially at higher test temperatures. Particularly at 40ºC, coarse aggregates seem to disturb mixture rearrangement due to compaction, which results in cracking.

Binder Content Effect

The binder content of slabs 2, 3 and 7 was 5.8%, 7.3% and 5.3%, respectively. Slab 7 showed little evidence of TDC and slab 3 showed no evidence of TDC at all. However, slab 2, which had the optimum binder content, exhibited a significant amount of TDC at the end of the test. Despite this, the actual depth of the cracks was similar in slabs 7 and 2, i.e., 7 mm and 10 mm, respectively. This means that reduced binder content increases the time to the first crack; however, in-depth cracking progression is faster.

Segregation Effect

Field cores extracted during the forensic part of the work showed coarse aggregates at the top and fine aggregates in the lower part of the wearing course. This was replicated in simulating segregation in the laboratory-prepared slabs. For the test performed at 50ºC, it was noticed that cracks were confined to the coarse-graded surface and did not progress to the lower finer-grained layer. On the other hand, the coarse-graded aggregate at the top reduced rutting, which likely influenced TDC (Figure 2 f).

Binder Type Effect

Slab 16 was produced with 35/50 penetration binder. This slab exhibited a significantly higher number of load passes to TDC initiation, compared to the 50/70 penetration binder, as is evident when comparing *nf* values for otherwise similar slabs tested at 50ºC, (e.g., slab 6).

Aggregate-Binder Adhesion Effect

It was noticed that TDC first initiated around coarse aggregates, which may be the result of poor adhesion between aggregate and binder. Hence, improving adhesion should mitigate this problem. For this purpose, an anti-stripping additive was used. As a result, crack opening tendency and rutting were reduced.

NUMERICAL SIMULATION

The laboratory experiment did provide an insight into the factors affecting TDC initiation; it was concluded that TDC is often associated with rutting. To further study the interaction between these two distresses, a numerical simulation was additionally undertaken in this study. It involved a 3-D non-linear dynamic finite element model to simulate the Wheel Tracking device. The Finite Element Program used was DIANA (17). The model geometry and the material characterization for this simulation are described hereafter.

Model Geometry Characterization

The 3D model dimensions were 30.0×15.0×7.0 cm (i.e., half test slab was analyzed due to symmetry). Twenty-node solid brick elements and rigid supports were used. Two meshes were used, one for the non-rutted surface and another for the rutted one. The non-rutted mesh is comprised of 378 elements and 2169 nodes, while the rutted mesh is comprised of 468 elements and 2600 nodes. Mesh base nodes were fixed in all directions and the lateral nodes were fixed only in the direction perpendicular to the boundary plane. Symmetry boundary plane nodes were fixed in the same way as the lateral nodes. Figure 3 shows the adopted mesh for the non-rutted geometry, as well as the loading configuration. Four sequential centered loading positions were considered. Each position was loaded with a pressure of 627 kPa in 8 time steps of 0.01455 s. The loaded area was equal to the contact area of the Wheel Tracking device wheel (i.e., 2.2×5.0/2 cm).

Material Characterization

Asphalt concrete models included a Burger's model, to describe viscoelastic behavior, and a constant stress cut-off smeared model, to describe cracking behavior. Material constants for these models were established through additional laboratory testing, as described below and summarized in Table 3.

Stiffness Modulus

Four point bending tests were performed to measure the stiffness modulus at 30ºC and 40ºC. It was also possible to test two specimens at 50ºC. Specimens, 38.0×6.5×5.0 cm in size, were extracted from each slab and submitted to sinusoidal loading, corresponding to a maximum strain, at the base, of 100 micro-strains. This was carried out

in the following decreasing order of frequency, namely 10, 5, 2, 1, 0.5, 0.2, and 0.1 Hz. Figure 4 shows the stiffness modulus and phase angle results.

As expected, the stiffness was lower, and phase angle was high, with increasing test temperatures. No difference was found, within the three temperature groups, due to the simulated construction variability.

Shear Modulus

An SST apparatus was used to determine the shear modulus at constant height, at temperatures of 30ºC, 40ºC and 50ºC. Two specimens with a 50 mm radius and 50 mm height, were extracted from each slab and submitted to sinusoidal loading resulting in a shear strain amplitude of 100 micro-strains, in the following decreasing order of frequency, namely 10, 5, 2, 1, 0.5, 0.2, 0.1, 0.05, 0.02 and 0.01 Hz. Figure 5 shows the shear modulus and phase angle results. The non-linear relationship between the logarithm of shear modulus and loading frequency, as well as between the logarithm of phase angle and loading frequency, is evident. At 30ºC and 40ºC the coarse and the fine graded mixtures possessed lower shear moduli compared to the other gradations. However, at a 50ºC, the mixture with the aggregate gradation C (i.e., slab 5) and B (i.e., slab 4) possessed the lower moduli. At 50ºC, the use of harder binder and the coarser aggregate resulted in higher shear modulus. The additive did not seem to affect the shear modulus.

Tensile Strength

The indirect tension test has been suggested in the literature as suitable to quantify cracking behavior (15, 16). This test was carried out by applying a compressive diametral load to a cylindrical specimen with a 50.05 mm radius and a 50.00 mm height at a controlled deformation rate of 51.00 mm per minute. Test temperature was 30ºC, 40ºC and 50ºC according to Table 1. Load and deflection were measured. Using this information, the tensile strength, as well as the fracture energy and the modulus, were determined (Table 4). Due to the high testing temperatures, the mixture responses were slightly non-linear before the maximum load was reached. Nevertheless, fracture energy (fracture energy$_{Lmax}$) was computed as the triangular area of the linear approximation of the stress versus deflection diagram. In terms of tensile strength, similar values were obtained for all the mixtures tested at the same temperature. The only exceptions were slabs 7 and 16, which yielded different strengths as a result of the different binder grades used. In terms of fracture energy, low values were found in high air void mixtures (i.e., slabs 1, 7 and 17) and vice-versa (i.e., slabs 3, 4 and 5).

Cyclic Compression Test

Cyclic compression tests were conducted to simulate traffic loading. They were carried out on cylindrical specimens (100 mm diameter and 70 mm height), at 30ºC, 40ºC and 50ºC, placed between two parallel loading platens. Each specimen was subjected to a cyclic axial square-pulse vertical stress at frequencies of 0.5 Hz and 100 kPa for 2 hours. No preload nor confinement pressure was applied. During the test, plastic and elastic axial deformations were measured at specified numbers of load applications.

This data was used to adjust mixture's viscoelastic properties, using a Burger's model. The linear part of the deflection-time curve was used to establish η_1 according to Equation 1. The remaining parameters were obtained in each loading cycle by adjusting Burger's theoretical time-deflection curve to better adjust the laboratory curves. Table 5 lists the mechanical constants adjusted to the cyclic compression data tested.

$$\eta_1 = \frac{\int_{t_0}^{t_1} \sigma(t)dt}{\Delta\varepsilon_{plastic}(t_0, t_1)} \quad (1)$$

Where

η_1 = Maxwell's dashpot constant,

$\sigma(t)$ = applied tension,

$\Delta\varepsilon_{plastic}$ = plastic deformation difference between time t_0 and t_1.

Important differences were found in the η_1 parameter between cores of the same slab and between slabs due to temperature effect. In general, results were according to those obtained by other authors. For the finite element

analysis, the Burger's model parameters adopted were the average values obtained for each temperature tested. These constants were frequency-shifted to model frequencies other than those tested.

Results of the Numerical Simulation

Analysis of Temperature Effect

TDC takes place when a conjunction of shear and normal stresses reaches a critical combination. Cracking can originate at or near the surface of the slab. Normal stresses were found to be predictably similar for the 3 temperatures simulated, while shear stresses seemed to increase with temperature. At 50ºC shear stresses seemed to exceed normal stresses in the vicinity of the load. Figure 6 shows the stress distribution, as well as the cracking generated when the wheel load is in position 4. In positions 1, 2 and 3 the shear stresses are seen to be higher than the normal tensile stresses. It is concluded that viscoelastic behavior plays an important role in TDC initiation.

Analysis of Rutting Effect

As pointed out earlier, the rutted pavement surface was modeled by reducing the slab thickness in the wheel path by 5 mm. As a result, the stress distribution changed significantly in the vicinity of the wheel path, surpassing its tensile strength at 40ºC and 50ºC. At 30ºC and 40ºC, shear stresses remained relatively constant, whereas at 50ºC they increased significantly (Figure 7). This explains why cracks were generated at 40ºC after a few more wheel passes. It is concluded that the stresses generated in response to the rutted geometry can be sufficient to initiate TDC at temperatures lower than those for a non-rutted geometry.

CONCLUSIONS

The work presented in this paper summarizes the results of a laboratory and modeling study of TDC initiation. The laboratory work involved Wheel Tracking tests of 17 mixtures that simulated the range of mixture characteristics established from an earlier forensic TDC study. These slabs were tested at three temperatures (30ºC, 40ºC and 50ºC). It was found that surface cracking initiated earlier at higher temperatures. The most important factors affecting TDC initiation were air voids (high air voids) and aggregate gradation (coarse aggregates). Modeling involved a 3-D non-linear viscoelastic finite element model, which accounted explicitly for the non-rutted and the rutted shape of the pavement surface. Modeling of the TDC involved laboratory testing to establish the viscoelastic and tensile strength properties of the asphalt mixtures tested. It was found that the rutted surface seems to contribute significantly to TDC initiation. The results provided a general vision of TDC initiation causes that may be used as guidelines in more specific research, which should consider a larger number of mixtures and samples in order to be enable the establishment of TDC behavior models.

REFERENCES

1. Komoriya, K., T. Yoshida and H. Nitta. *"WA-DA-CHI-WA-RE" Surface Longitudinal Cracks on Asphalt Concrete Pavement*. CD-ROM. Transportation Research Board 80th Annual Meeting. Washington, D.C., 2001.
2. Myers L.A. *Development and Propagation of Surface Initiated Longitudinal Wheel Path Cracks in Flexible Highway Pavements*. PhD. Thesis. University of Florida. Florida, 2000.
3. Matsuno, S. and T. Nishizawa. *Mechanism of Longitudinal Surface Cracking in Asphalt Pavement*. 7th International Conference on Asphalt Pavements. Volume 2. University of Nottingham, 1992, pp 277-291.
4. Freitas, E., P. Pereira and L. Picado-Santos. *Top-Down Cracking Study* (in Portuguese). Estrada 2002. 2º Congresso Rodoviário Português. Lisboa, 2002, pp 319-330.
5. Merrill, D.B. *Investigating the Causes of Surface Cracking in Flexible Pavements Using Improved Mathematical Models*. PhD. Thesis. Department of Civil Engineering. University of Wales Swansea. Wales, 2000.
6. Groenendijk, J. *Accelerated Testing and Surface Cracking of Asphaltic Concrete Pavements*. PhD. Thesis. Delft, 1998.
7. Myers, L.A., R. Roque and B. Birgisson. *Propagation Mechanisms for Surface-Initiated Longitudinal Wheel Path Cracks*. Transportation Research Record 1778. Transportation Research Board. Washington, D.C., 2001, pp 113-122.
8. Uchida K., T. Kurokawa, K. Himeno and T. Nishizawa. *Healing Characteristics of Asphalt Mixture Under High Temperature Conditions.* CD-ROM. Ninth International Conference on Asphalt Pavements. Copenhagen, 2002.

9. Uhlmeyer, J.S., K. Willoughby, L.M. Pierce and J. Mahoney. *Top-Down Cracking in Washington State Asphalt Concrete Wearing Courses*. Issues in Pavement Design and Rehabilitation. Transportation Research Record No. 1730. Transportation Research Board. Washington D.C., 2000, pp 110-116.
10. Svasdisant, T., M. Achorsch, G. Baladi and S. Pinyosunun. *Mechanistic Analysis of Top-Down Cracking in Asphalt Pavements.* CD-ROM. 81st Transportation Research Board Annual Meeting. Washington D.C., 2002.
11. Freitas, E., P. Pereira and L. Picado-Santos. *Assessment of Top-Down Cracking Causes in Asphalt Pavements.* 3rd International Symposium on Maintenance and Rehabilitation of Pavements and Technological Control. Guimarães, Portugal, 2003, pp 555-564.
12. Schorsch, M., C. Chang and Y. Baladi. Effects *of Segregation on the Initiation and Propagation of Top-Down Cracks.* CD-ROM. Transportation Research Board 82nd Annual Meeting. Washington, D.C., 2003.
13. Duriez M. *Traité de Materiaux de Construction*. Dunot. Paris, 1950.
14. Wang, L., L.A. Myers and L. Mohammad. *A Micromechanics Study on Top-Down Cracking*. CD-ROM. Transportation Research Board 82nd Annual Meeting. Washington, D.C., 2003.
15. Roque, R. and W. Buttlar. *The Development of a Measurement and Analysis System to Accurately Determine Asphalt Concrete Properties Using the Indirect Tensile Mode*. Journal of the Association of Asphalt Paving Technologists. Volume 61, 1992, pp 304-332.
16. Martinez, F. and S. Angelone. *Determination of Fracture Parameters of Asphalt Mixes by the Repeated Indirect Tensile Test*. Sixth RILEM Symposium. Zurique, 2003, pp 387- 393.
17. DIANA Online Users Manual, Release 8.1, TNO Building and Construction Research, Delft, Netherlands, 2003.

LIST OF TABLES

LIST OF FIGURES

TABLE 1 Slab characteristics

Parameter	Slab Number																
	1	2	3	4	5	6	7	8	9	10	11	12	13	14	15	16	17
Grading (A, B, C)	A	A	A	B	C	A	A	A	A	A	B	C	A	A	A	A	A
Density (g/cm^3)	2.24	2.32	2.34	2.33	2.31	2.30	2.26	2.32	2.29	2.31	2.30	2.30	2.30	2.30	2.31	2.27	2.24
Void Content (%)	8.2	4.1	2.1	4.1	4.6	5.6	7.8	4.1	4.4	3.8	3.2	4.9	4.6	3.8	4.2	6.6	7.8
Bitumen Content (%)	5.7	5.8	7.6	6.1	5.8	5.8	5.3	5.7	5.8	5.8	6.1	5.8	5.8	5.8	5.3	5.8	5.8
Bitumen Type (1:50/70; 2:35/50)	1	1	1	1	1	1	1	1	1	1	1	1	1	1	1	2	1
Addictive ($^0/_{00}$)	0	0	0	0	0	0	0	0	0	0	0	0	0	0	0	0	3
Segregation (yes, no)	no	no	no	no	no	no	no	no	no	no	no	no	yes	yes	no	no	yes
Temperature (ºC)	50	50	50	50	50	50	50	30	50	40	30	40	50	30	40	50	50

TABLE 2 Number of wheel passes

Slab Number	Temperature	nf	nt
1	50ºC	500	2880
2	50ºC	645	6868
3	50ºC	344	1763
4	50ºC	860	4042
5	50ºC	-	5917
6	50ºC	860	7614
7	50ºC	1300	10000
9	50ºC	860	4200
13	50ºC	650	2947
16	50ºC	2150	10300
17	50ºC	9800	10274
10	40ºC	6250	12550
12	40ºC	1075	10000
15	40ºC	1075	10000
8	30ºC	7700	19318
11	30ºC	> 16500	19136
14	30ºC	> 10000	16063

TABLE 3 Properties adopted in FEM simulation

Temperature (ºC)	E1 (MPa)	E2 (MPa)	$\eta 1$ (MPa.s)	$\eta 2$ (MPa.s)	μ	σ_t (MPa)
30	2100	400	50000	130	0.35	0.50
40	500	300	16000	85	0.40	0.25
50	200	300	6800	80	0.48	0.15

TABLE 4 Summary of results obtained by tensile stress tests

Slab Number	Temperature (ºC)	$Load_{max.}$ (N)	Stress (MPa)	$Deflection_{Lmax}$ (mm)	$Fracture\ Energy_{Lmax}$ (MPa×mm)	Modulus (MPa)
8	30	3839	0.501	2.8	0.704	17.832
11	30	3807	0.487	4.0	0.974	12.173
14	30	3578	0.467	3.3	0.775	14.067
10	40	1926	0.259	2.4	0.312	10.741
12	40	1662	0.218	3.8	0.411	5.777
15	40	1853	0.248	2.2	0.270	11.375
1	50	924	0.119	2.2	0.129	5.491
2	50	1030	0.132	2.4	0.159	5.443
3	50	888	0.117	5.4	0.318	2.151
4	50	1049	0.139	5.8	0.401	2.398
5	50	1016	0.132	4.8	0.319	2.723
6	50	1042	0.136	3.8	0.256	3.606
7	50	1223	0.157	2.8	0.218	5.671
9	50	1088	0.140	3.7	0.257	3.798
13	50	996	0.128	3.7	0.235	3.476
16	50	1637	0.209	3.6	0.377	5.815
17	50	1073	0.139	3.6	0.250	3.859

TABLE 5 Burger's model parameters

Slab Number	E1 (MPa)		E2 (MPa)		η1 (MPa.s)		η2 (MPa.s)	
Specimen	A	B	A	B	A	B	A	B
1	99	130	270	476	1315	6427	69	118
2	137	133	446	365	5863	4079	116	90
3	-	-	-	-	-		-	-
4	131	131	344	325	6276	5285	104	97
5	131	118	395	330	10342	7692	100	93
6	167	236	232	300	15603	8758	55	59
7	120	111	348	411	5553	4813	86	96
8	183	220	356	430	46203	52371	123	146
9	123	133	245	408	18796	4355	89	120
10	146	147	232	345	16212	13061	77	103
11	-	213	-	498	-	24202	-	159
12	165	155	279	265	16444	20667	78	75
13	123	-	351	-	3249	-	95	-
14	208	135	390	193	42455	64964	124	77
15	143	164	317	289	11369	15970	96	83
16	141	144	405	288	13675	8063	98	97
17	131	116	299	289	8121	5062	84	82

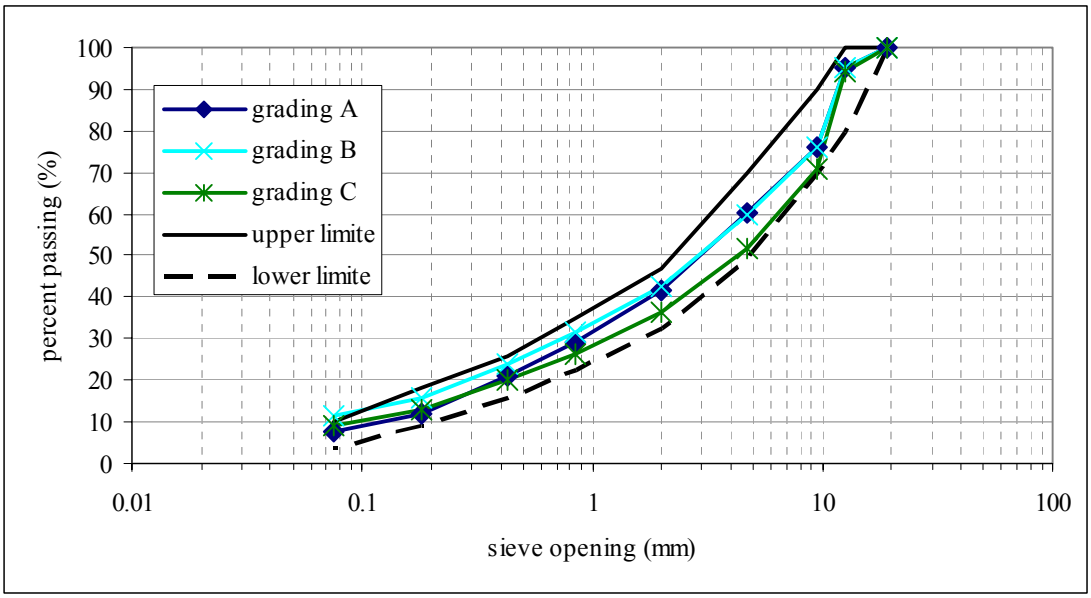

FIGURE 1 Grading curves and grading envelope

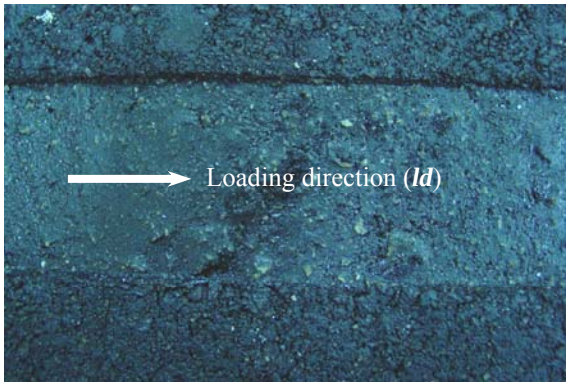

a) Slab 8; 30ºC; nt = 19318 (plan view)

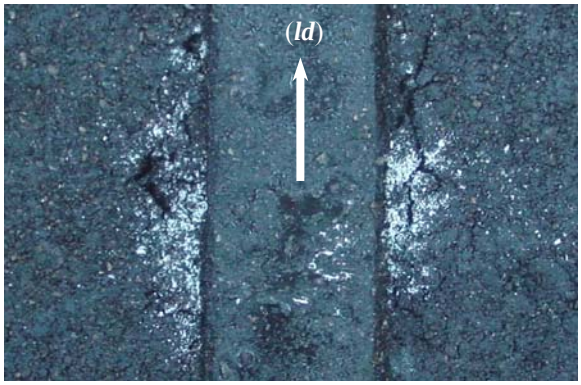

d) Slab 1; 50ºC; nt = 2880 (plan view)

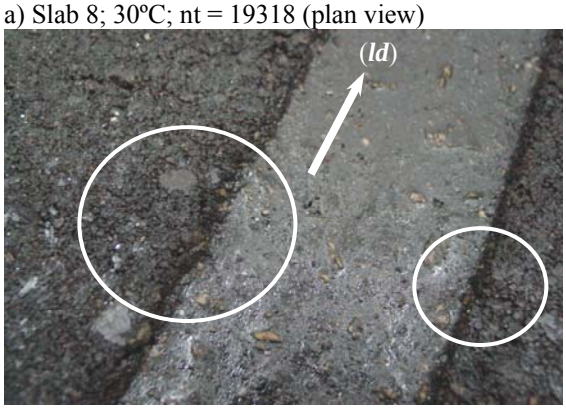

b) Slab 10; 40ºC; nt = 12550 (plan view)

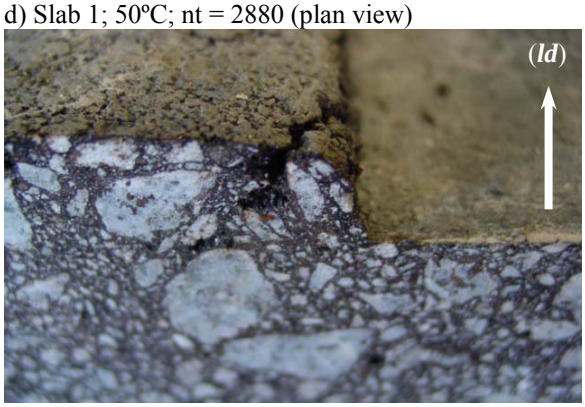

e) Slab 7; 50ºC; nt = 10000 (side view)

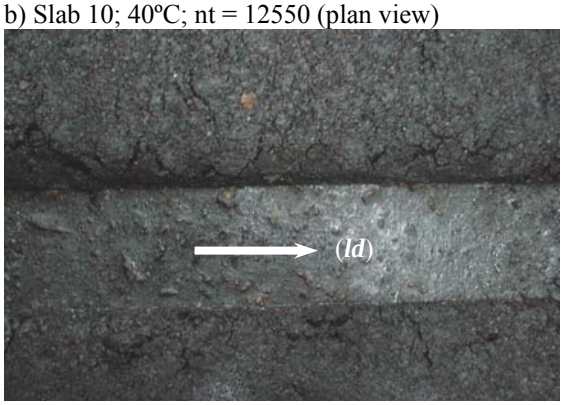

c) Slab 2; 50ºC; nt = 6868 (plan view)

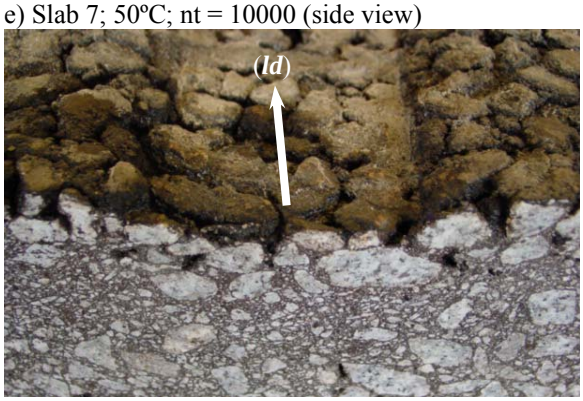

f) Slab 17; 50ºC; nt = 10274 (side view)

FIGURE 2 Slabs condition after wheel tracking test

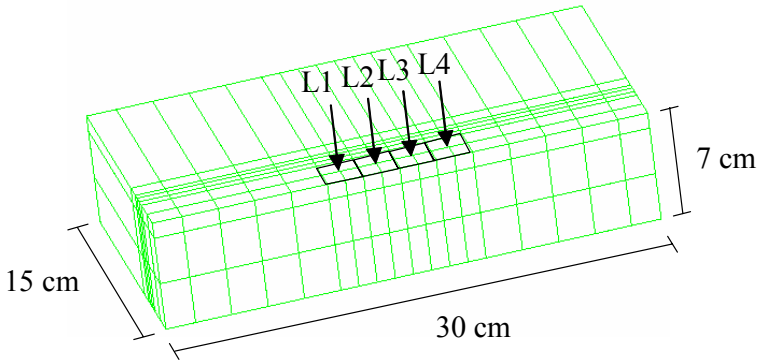

FIGURE 3 Adopted mesh

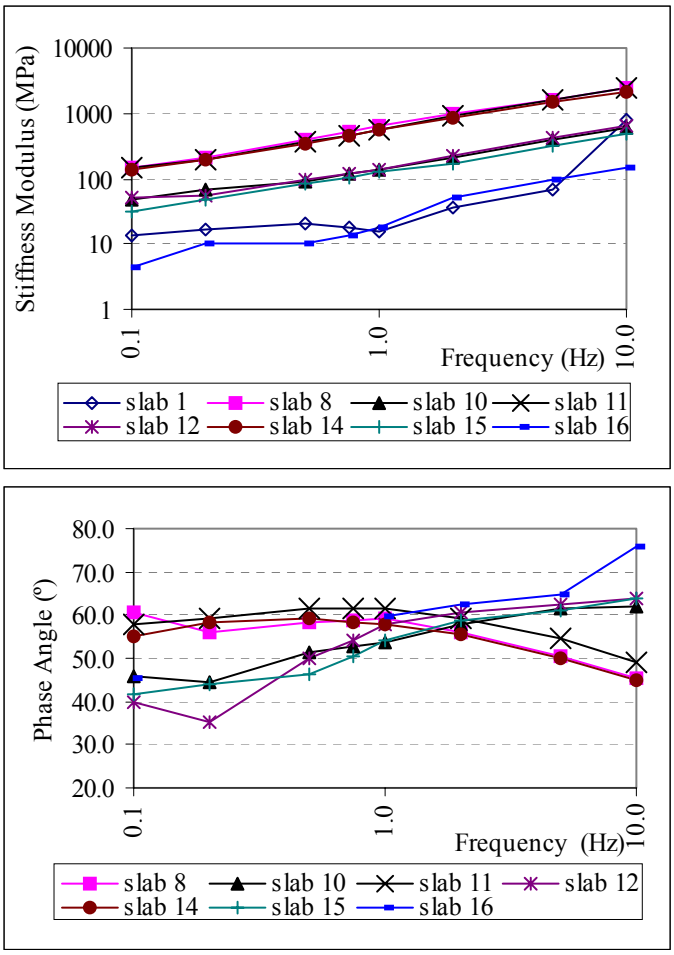

FIGURE 4 Stiffness modulus and phase angle

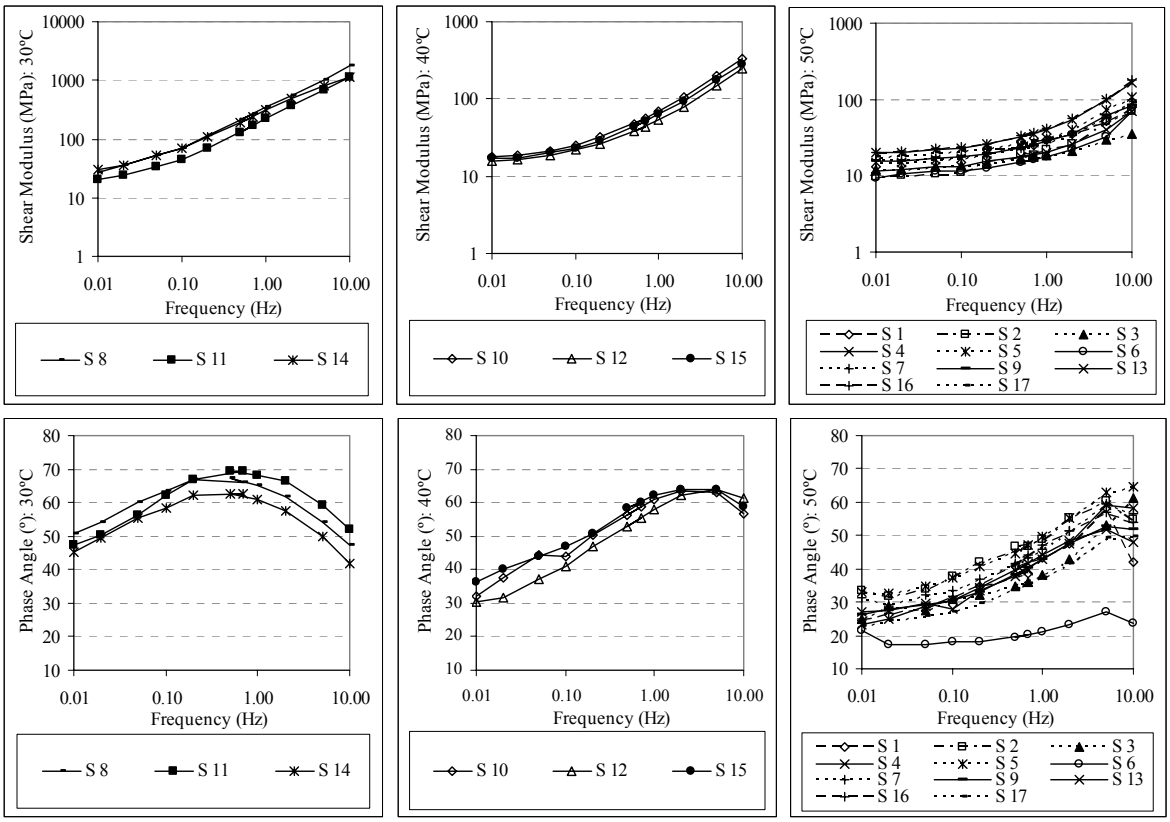

FIGURE 5 Shear modulus and phase angle

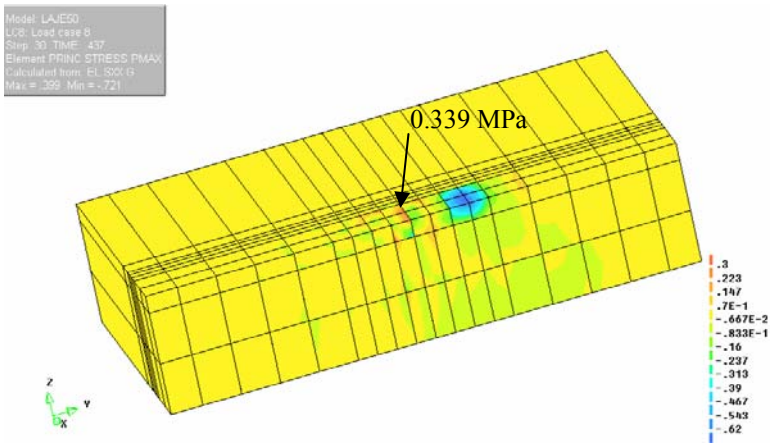

a) Maximum principal stress (P1)

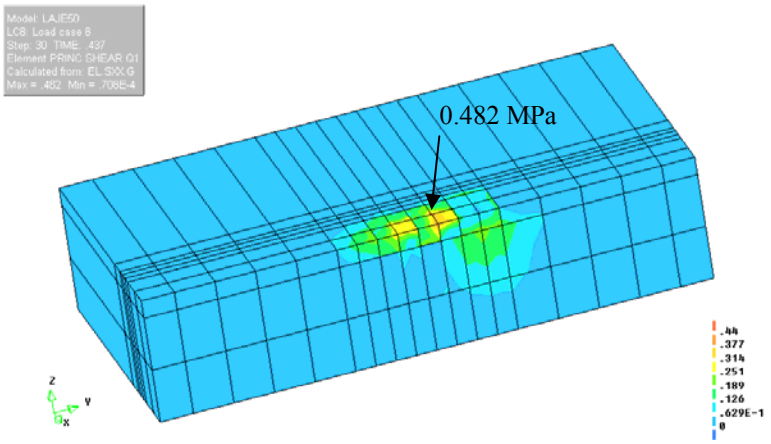

b) Maximum shear stress (Q1)

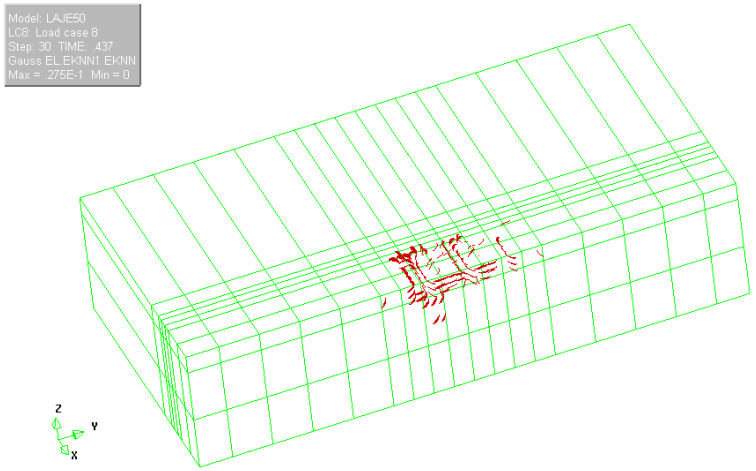

c) Cracking

FIGURE 6 Stresses and total cracking generated in loading position 4 (50ºC)

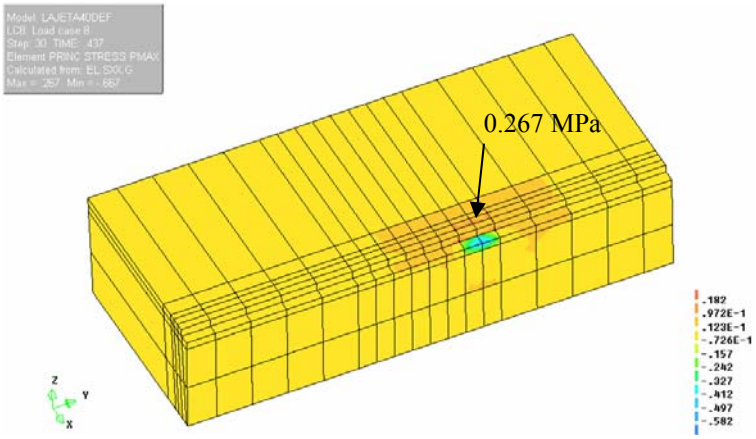

a) Maximum principal stress (P1), T = 40ºC

(view near wheel track edge)

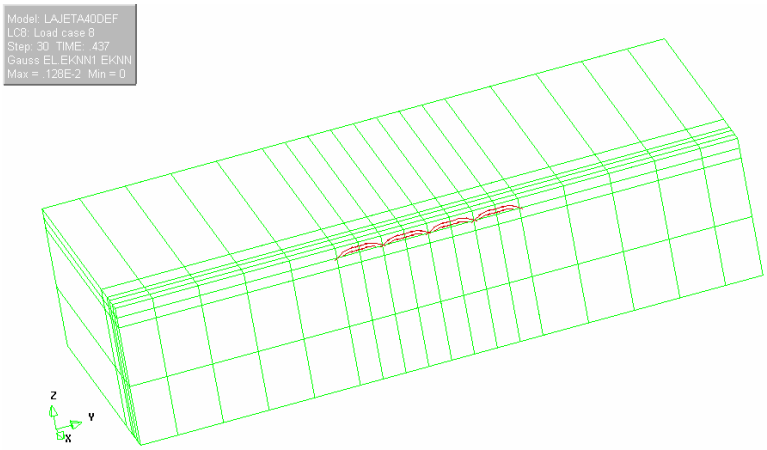

c) Cracking, T = 40ºC (view near wheel track edge)

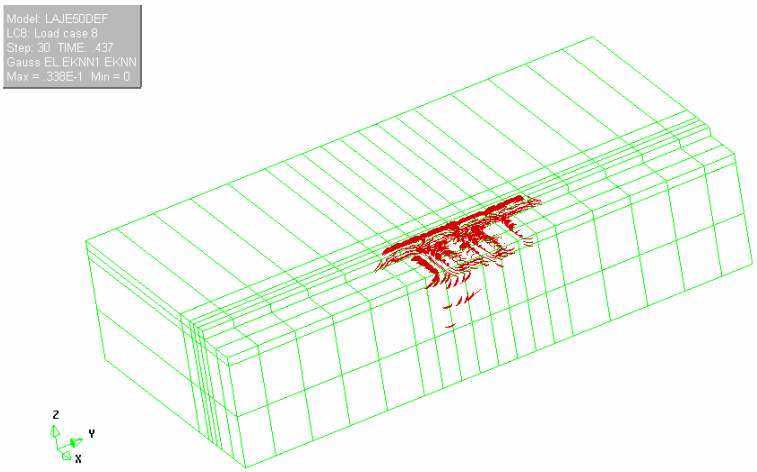

c) Cracking, T = 50ºC

FIGURE 7 Stresses and cracking due to rutting in loading position 4